

RESEARCH ARTICLE

Limb bone strains during climbing in green iguanas (*Iguana iguana*): testing biomechanical release as a mechanism promoting morphological transitions in arboreal vertebrates

V. David Munteanu^{1,*}, Kelly M. Diamond² and Richard W. Blob¹

ABSTRACT

Across vertebrate diversity, limb bone morphology is typically expected to reflect differences in the habitats and functional tasks that species utilize. Arboreal vertebrates are often recognized to have longer limbs than terrestrial relatives, a feature thought to help extend the reach of limbs across gaps between branches. Among terrestrial vertebrates, longer limbs can experience greater bending moments that might expose bones to a greater risk of failure. However, changes in habitat or behavior can impose changes in the forces that bones experience. If locomotion imposed lower loads in trees than on the ground, such a release from loading demands might have produced conditions under which potential constraints on the evolution of long limbs were removed, making it easier for them to evolve in arboreal species. We tested for such environmental differences in limb bone loading using the green iguana (*Iguana iguana*), a species that readily walks over ground and climbs trees. We implanted strain gauges on the humerus and femur, and then compared loads between treatments modeling substrate conditions of arboreal habitats. For hindlimbs, inclined substrate angles were most correlated with strain increases, whereas the forelimbs had a similar pattern but of lesser magnitude. Unlike some other habitat transitions, these results do not support biomechanical release as a mechanism likely to have facilitated limb elongation. Instead, limb bone adaptations in arboreal habitats were likely driven by selective pressures other than responses to skeletal loading.

KEY WORDS: Locomotion, Biomechanics, Lizard, Limb bone, Arboreality

INTRODUCTION

Morphological diversity across the skeletal elements of vertebrate species is often viewed as relating to differences in their mechanical function (Wainwright et al., 2005; Aiello et al., 2017). One factor contributing to such views is the role of skeletons as load-bearing structures (Turner and Pavalko, 1998). Changes in shape can impact the ability of a structure to bear loads (Lieberman et al., 2004; McHenry et al., 2006; Rivera and Stayton, 2011), and changes in use have the potential to impact the loads to which a structure is


exposed, potentially making changes in bone shape advantageous (e.g. Blob and Biewener, 1999; Iriarte-Díaz, 2002; Young and Blob, 2015). For example, changes in behavior or habitat can lead to increases in the loads to which a structure is exposed (Kemp et al., 2005; Byron et al., 2011; Granatosky et al., 2018). In the short term, processes of bone modeling and remodeling can elevate limb bone density in response to higher loading, as seen in martial arts practitioners (Ito et al., 2016) and the dominant arms of tennis players (Calbet et al., 1998). Shifts to locomotion that involves frequent turning have also been correlated with changes in the cross-sectional shape of the femur in mice (Carlson and Judex, 2007). However, this perspective can also be extended into evolutionary time scales. For example, pit bull dogs (exposed to selection for fighting prowess by humans) showed robust bones suited to resist high forces incurred during fighting (Kemp et al., 2005). In this case, the addition of elevated loads may have made particular structural features of the limbs advantageous for pit bulls, such that selection (imposed by humans) favored a distinct morphology for the limb bones.

Beyond increases in loading, however, an additional perspective is that changes in environment may remove specific loading demands on the skeleton and, thereby, potentially open opportunities for morphological diversification through a kind of biomechanical release. For example, among swimming turtles, the reduction of torsional strains during aquatic propulsion has been proposed to have removed specific advantages of tubular-shaped limb bones for resisting such loads (Young and Blob, 2015; Young et al., 2017). With reduced demand for resistance to torsion it became possible for nontubular limb bone shapes to evolve, potentially enabling the eventual evolution of flattened limb bones among species that flap their limbs to swim, such as sea turtles (Young and Blob, 2015; Young et al., 2017). This specific evolutionary transition was associated with a lineage that shifted from terrestrial to aquatic habitats. Could it also be possible for changes in skeletal loading to help explain changes in limb shape across evolutionary transitions between other types of habitats?

Arboreal vertebrates have been described as having limb bones that are typically longer than those of closely related species that live mainly on the ground (Cartmill, 1985; Herrel et al., 2013; Kilbourne and Hoffman, 2015; Meldrum et al., 1997; Rooney, 2018). Although elongate limbs are considered advantageous during climbing to extend reach between grips (Cartmill, 1985), longer limbs would also have greater moment arms for applied bending forces and would be expected to incur elevated bending loads during terrestrial locomotion (Biewener, 1983). Moreover, the limbs of arboreal taxa may have significantly different loading patterns than those of terrestrial relatives (Demes and Carlson, 2009; Lammers and Gauntner, 2008). A particularly distinctive example of an arboreal species from which skeletal loads have been

¹Department of Biological Sciences, Clemson University, Clemson, SC 29634, USA. ²Department of Biology, Rhodes College, Memphis, TN 38112, USA.

*Author for correspondence (munteanu.david@gmail.com)

 V.D.M., 0000-0002-0318-2423; K.M.D., 0000-0001-8639-6795; R.W.B., 0000-0001-5026-343X

This is an Open Access article distributed under the terms of the Creative Commons Attribution License (<http://creativecommons.org/licenses/by/4.0>), which permits unrestricted use, distribution and reproduction in any medium provided that the original work is properly attributed.

evaluated is the gibbon (*Hylobates lar*), in which recordings have been made from strain gauges implanted on the ulna, radius and humerus during brachiation (Swartz et al., 1989). These data showed that the elongated limb bones of *H. lar* experienced high tensile loads, which are unusual among vertebrate limb bones (Biewener, 1990). Because the body is suspended from the limbs rather than supported by them during brachiation, tensile loading might not be expected among elongated limb bones of arboreal vertebrates more generally. However, it is also possible that, rather than elevation of specific types of loads promoting particular skeletal morphologies in arboreal taxa, a decrease in dominant loading regimes could open opportunities for a diversification of limb bone shapes (Young and Blob, 2015). For example, animals climbing vertical surfaces or steep inclines might actually be pulled off of those surfaces by gravity (Autumn et al., 2006; Maie et al., 2012), which could reduce the standard compressive or bending loads that such animals would experience during the support of body weight on level ground. Gravity might also pull climbing animals off of steep inclines, changing strain profiles on their limb bones in a similar fashion. In addition, compliance of arboreal substrates such as branches might also reduce overall load magnitudes to which limb bones are exposed, such that elongated limb bones might not incur disadvantageous levels of bending and, therefore, have an increased potential to persist through the course of evolution, were they to appear.

In this study, we used bone strain measurements from the forelimbs and hindlimbs of green iguanas to test for differences in limb bone loading during climbing compared with level locomotion. Through these measurements, we evaluated whether climbing produces patterns of skeletal loading consistent with expectations based on differences in limb morphology between arboreal and more terrestrial taxa, and whether biomechanical release from loading might have been a viable mechanism to have contributed to such changes.

MATERIALS AND METHODS

Animal collection and husbandry

Fourteen *Iguana iguana* (Linnaeus 1758) [snout–vent length (SVL) 28–37 cm; mass 0.86–2.05 kg] were collected from Palm Beach County, FL, USA, using pole and lasso, and were transported by car to our home lab facility in Clemson, SC, USA. Housing and husbandry followed published standards (Hatfield, 1996) and Clemson IACUC requirements (AUP 2017-071 and 2018-041). Animals were housed in a greenhouse within large plastic enclosures (cattle tanks with wire mesh lids: 147×100×52 cm, length×width×height) fitted with climbing surfaces, basking areas and shelters to promote activity and enrichment. Temperatures were kept between 27 and 37°C with an ambient light:dark cycle and full spectrum lighting via direct sunlight provided by moveable panels in the greenhouse roof. Animals were supplied with water *ad libitum*, and were fed daily with a mix of collard greens, carrots and mangoes, supplemented with a vitamin/mineral powder.

Surgical procedures

To conduct strain recordings, one rosette (FRA-1-11) and two single element (FLK-1-11) strain gauges (Tokyo Sokki Kenkyujo Co., Ltd., Japan) were surgically implanted onto the midshaft of one proximal limb bone for each iguana (right femur, $n=6$; right humerus, $n=8$), using aseptic technique. Techniques were based on procedures detailed in Blob and Biewener (1999). Anesthesia was induced by intramuscular injections of 60–100 mg kg⁻¹ ketamine and 1 mg kg⁻¹ xylazine into the left M. triceps brachii (Romer,

1922), with analgesia provided through an injection of 1 mg kg⁻¹ butorphanol at the same site. For animals with lower initial doses of ketamine, additional injections of up to 40 mg kg⁻¹ were given if a surgical plane of anesthesia was not achieved.

To implant the strain gauges, a longitudinal incision was made along the medial surface of the thigh or arm. For individuals in which femoral strains were measured, the M. iliotibialis, M. femorotibialis and M. ambiens were gently separated along fascial planes and retracted to expose the surface of the femur; for individuals in which humeral strains were measured, the M. biceps humerus and M. brachialis inferior were separated and retracted to expose the humerus (Romer, 1922). At sites selected for implantation, the periosteum was removed by gentle scraping with a periosteal elevator, and the bone surface was swabbed clean with diethyl ether and allowed to dry for several seconds. Gauges were attached at midshaft to each bone using self-catalyzing cyanoacrylate adhesive (Duro™ Superglue; Henkel Loctite Corp., Avon, OH, USA). For the femur, rosette gauges were attached to the dorsal surface, and two single element gauges were attached to the anterior and ventral surfaces, respectively. Gauges were attached to the humerus in a similar distribution, but with the rosette placed on the anterior surface and single element gauges placed in ventral and posteroventral positions. After the gauges were attached, lead wires (336 FTE, etched Teflon; Measurements Group, Raleigh, NC, USA) were passed subcutaneously to an incision made dorsal to the hip (femur) or the glenohumeral joint (humerus), where they exited the limb. Incisions were then sutured closed, and gauge wire contacts were soldered into a microconnector and secured with epoxy adhesive. Self-adhesive bandage was then wrapped around the exposed length of the lead wires to protect them and allow them to be secured as a cable to either the hip or shoulder region. Individuals were given 24 h to recover from surgery and qualitatively assessed for recovery of normal limb function before experimental trials commenced.

Strain data collection and analysis

The day following surgery, locomotor trials were conducted with each iguana in a wooden trackway (243×56×49 cm, length×width×height) with a clear Plexiglas panel on one side that allowed filming of trials. The trackway could be adjusted to simulate five environmental conditions, each of which was assigned an abbreviation as a naming convention: (1) a level trackway with a flat, non-compliant surface, simulating standard terrestrial substrates (FL-LEV); (2) a flat, non-compliant trackway angled at a 65 deg incline (Fig. 1), simulating the substantial deviation from horizontal of many tree trunks, particularly those growing over riverbanks common in the natural habitat of iguanas in Florida (FL-INC); (3) a level trackway with a compliant surface, formed by inserting a flexible (0.3 cm thick) plywood sheet over the entirety of the trackway that could flex 7.5 cm at its midpoint between end supports that were 8.9 cm tall, simulating the compliance of branches found in many arboreal habitats (FL-COMP); (4) a level trackway with a curved surface, constructed from 30 cm diameter PVC pipe that was bisected longitudinally, laid along the length of the flat trackway, simulating the curvature of tree trunks (CRV-LEV); and (5) a trackway inclined at 65 deg, with the curved surface inserted (CRV-INC). For all trackway conditions, a 3-mm-thick foam exercise mat was attached over all of the contact surfaces to improve grip of the iguanas' feet and limit slipping or sliding during locomotion. Trials across these different conditions allowed distinct consideration of the effects of different features of arboreal habitats on limb bone loading, including surface inclination, compliance and geometry. Each animal was tested in each condition until strains were recorded from ~20

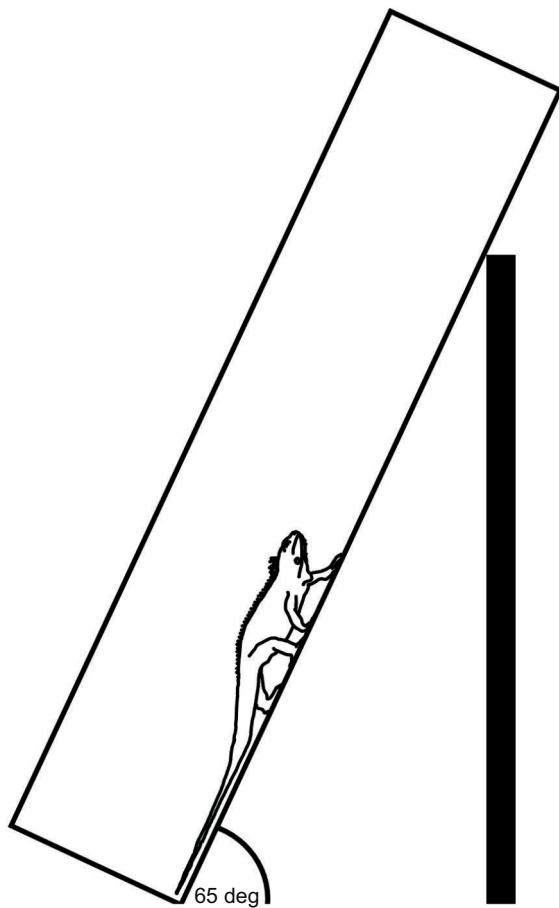


Fig. 1. Schematic of trackway representing the 65 deg incline (flat-incline, FL-INC) condition.

steps. However, the order of test conditions was randomized across animals. Owing to strain gauge failures, useable data were ultimately collected from the femur of five individuals and the humerus of six individuals. In addition, failure of some gauges partway through experiments meant that for such gauges, a full set of 20 strain values could not be collected for each locomotor condition (see Tables S1 and S2 for sample sizes of steps for each gauge, per individual and condition).

To collect strain signals, the microconnectors were connected to Vishay conditioning bridge amplifiers (model 2120B; Measurements Group) via a shielded cable. Raw voltage signals were sampled through an A/D converter (PCI6031E; National Instruments Corp., Austin, TX, USA) at 2500 Hz, saved to a computer using data acquisition code written in LabVIEW™ (v. 6.1, National Instruments) and calibrated to microstrain ($\mu\epsilon = \text{strain} \times 10^{-6}$) for each recording session via 1000 $\mu\epsilon$ toggle switches on the amplifiers. Trials were conducted to encourage a consistent speed across batches of one to four steps. Although speeds may not have been strictly dynamically equivalent across different conditions (e.g. level versus inclined), they still provide data with comparable ecological relevance for understanding selection pressures on skeletal morphology. Strain trials were filmed from the lateral perspective (120 Hz; GoPro Hero 3, GoPro, San Mateo, CA, USA). Video data were synchronized with strain data using a trigger connected to an LED visible in the camera frames, which simultaneously produced 1.5 V pulses visible in one

of the channels of the strain recordings. Video frames marking the start and end of footfalls, as well as the time of the light pulse, were determined using Adobe Premiere Pro™. At the completion of all trials for an individual, each iguana was euthanized (Beuthanasia®-D pentobarbital sodium solution; Merck Animal Health, Millsboro, DE, USA; 200 mg kg⁻¹ intraperitoneal injection) and frozen for later dissection of limb elements.

Conventions for the analysis and interpretation of strain data closely followed previous studies of skeletal loading in reptiles (Blob and Biewener, 1999; Butcher et al., 2008; Sheffield et al., 2011; Young et al., 2017). For each step, peak strain values for each axially aligned recording channel were extracted. In addition, shear strain magnitudes, and magnitudes and orientations of peak principal strains (i.e. maximum and minimum strains at each site, regardless of alignment with the long axis of the limb bone), were calculated from the output of the three rosette gauge channels following published methods (Carter, 1978; Dally and Riley, 1991; Biewener and Dial, 1995). Values of principal tensile strain orientations (ϕ_t) and shear strain magnitudes provided insight into the importance of torsional loading: with the long axis of each bone defined as 0 deg (and the perpendicular axis defined as 90 deg), pure torsion would be reflected by a ϕ_t orientation of 45 deg.

To simplify comparisons between trackway conditions, each condition was separated into three different factors: angle (level versus inclined), stiffness (stiff versus compliant) and curvature (flat versus curved). To compare the effect of trackway condition on each strain metric (axial strain maximum and minimum for each gauge, principal tensile strain, principle compressive strain and shear strain), we used a linear mixed-effects model in the packages ‘lme4’ and ‘lmerTest’ in R Statistical Software Version 4.2.1 (<https://www.r-project.org/>). We treated trackway factors angle, stiffness, curvature and body mass as fixed effects, and treated the individual animals as random effects. Type III ANOVA tests were performed to determine how each individual animal and each interacting trackway factor affected each of the strain variables (Table 1).

Cross-sectional analysis

An implanted femur and an implanted humerus (each bone from a different animal) were excised, cleaned and embedded in Bondo® Fiberglass Resin (3M, Maplewood, MN, USA). After curing, transverse sections were cut through each embedded bone at the location of the midshaft gauges. Photos of cross-sections were taken with a dissecting scope (ZEISS Stemi 508, Carl Zeiss Microscopy), Microsoft PowerPoint was used to trace the endosteal and periosteal margins and mark the locations of gauges, and the tracings were saved as JPEG files. These geometric data, along with the values of strain magnitude from the three recording locations, were input into analysis macros for NIH Image for Macintosh (<http://rsb.info.nih.gov/nih-image/>) to calculate the location of the neutral axis (NA) of bending and the planar distribution of longitudinal strains through femoral cross-sections (Lieberman et al., 2004). In a subset of steps, planar strain distributions were calculated at three time points (15%, 40% and 60% of stance) to evaluate shifts in the location and orientation of the NA throughout stance phase.

RESULTS

In each animal, the implanted gauges allowed a potential for nine strain magnitude variables to be compared across substrate conditions: maximum and minimum longitudinal strain magnitudes from each of the two single element gauges and the axial element of

Table 1. Significant individual and interacting trackway factor influence on hindlimb and forelimb strain metrics

| | Factor | d.f. | F | P |
|-----------------------------|----------------------|--------|--------|--------|
| Hindlimb | | | | |
| Maximum SE-R – dorsal | Angle | 1, 330 | 35.196 | <0.001 |
| | Angle:mass | 1, 329 | 50.869 | <0.001 |
| | Angle:curvature:mass | 1, 328 | 3.984 | 0.047 |
| Minimum R-pC | Angle | 1, 268 | 22.075 | <0.001 |
| | Angle:curvature | 1, 266 | 10.781 | 0.001 |
| | Angle:mass | 1, 267 | 32.732 | <0.001 |
| | Angle:curvature:mass | 1, 266 | 12.255 | <0.001 |
| Maximum SE – ventral | Angle | 1, 292 | 14.937 | <0.001 |
| | Stiffness | 1, 293 | 6.328 | 0.012 |
| | Angle:mass | 1, 294 | 12.143 | <0.001 |
| | Stiffness:mass | 1, 293 | 5.245 | 0.023 |
| Minimum SE – ventral | Angle | 1, 289 | 16.872 | <0.001 |
| | Curvature | 1, 294 | 7.790 | 0.006 |
| | Angle:curvature | 1, 293 | 8.354 | 0.004 |
| | Angle:mass | 1, 292 | 28.015 | <0.001 |
| | Curvature:mass | 1, 293 | 11.937 | <0.001 |
| | Angle:curvature:mass | 1, 293 | 10.569 | 0.001 |
| Maximum SE – anterior | Angle | 1, 204 | 40.386 | <0.001 |
| | Curvature | 1, 331 | 4.126 | 0.043 |
| | Angle:mass | 1, 249 | 30.460 | <0.001 |
| Minimum SE – anterior | Angle | 1, 334 | 4.948 | 0.027 |
| Forelimb | | | | |
| Maximum SE-R – anterior | Angle | 1, 314 | 59.346 | <0.001 |
| | Curvature | 1, 314 | 11.581 | <0.001 |
| | Angle:curvature | 1, 313 | 15.193 | <0.001 |
| | Angle:mass | 1, 314 | 43.746 | <0.001 |
| | Curvature:mass | 1, 314 | 13.754 | <0.001 |
| | Angle:curvature:mass | 1, 313 | 16.716 | <0.001 |
| Minimum R-pC | Stiffness | 1, 269 | 14.913 | <0.001 |
| | Angle:curvature | 1, 269 | 7.655 | 0.006 |
| | Stiffness:mass | 1, 269 | 12.270 | <0.001 |
| | Angle:curvature:mass | 1, 270 | 6.873 | 0.009 |
| Maximum R-pT | Angle | 1, 270 | 3.994 | 0.047 |
| | Curvature | 1, 270 | 24.148 | <0.001 |
| | Stiffness | 1, 269 | 12.538 | <0.001 |
| | Angle:curvature | 1, 270 | 46.013 | <0.001 |
| | Angle:mass | 1, 270 | 11.463 | <0.001 |
| | Curvature:mass | 1, 270 | 31.791 | <0.001 |
| | Stiffness:mass | 1, 269 | 11.813 | <0.001 |
| | Angle:curvature:mass | 1, 270 | 48.462 | <0.001 |
| | Stiffness | 1, 269 | 16.804 | <0.001 |
| | Angle:curvature | 1, 269 | 12.108 | <0.001 |
| Maximum R-shear | Stiffness:mass | 1, 269 | 14.942 | <0.001 |
| | Angle:curvature:mass | 1, 269 | 10.837 | 0.001 |
| | Curvature | 1, 513 | 7.329 | 0.007 |
| | Angle:curvature | 1, 513 | 4.561 | 0.033 |
| Maximum SE – posteroventral | Curvature:mass | 1, 513 | 8.737 | 0.003 |
| | Angle:curvature:mass | 1, 513 | 13.009 | <0.001 |
| | Curvature | 1, 512 | 8.653 | 0.003 |
| Minimum SE – posteroventral | Angle:curvature | 1, 512 | 5.405 | 0.020 |
| | Curvature:mass | 1, 512 | 5.035 | 0.025 |
| | Stiffness:mass | 1, 512 | 4.572 | 0.033 |
| | Angle:curvature:mass | 1, 512 | 5.093 | 0.024 |
| | Angle | 1, 315 | 9.609 | 0.002 |
| | Curvature | 1, 315 | 12.713 | <0.001 |
| Maximum SE – ventral | Mass | 1, 166 | 8.346 | 0.004 |
| | Angle:curvature | 1, 315 | 13.778 | <0.001 |
| | Angle:mass | 1, 315 | 11.621 | <0.001 |
| | Curvature:mass | 1, 315 | 13.201 | <0.001 |
| | Angle:curvature:mass | 1, 315 | 14.204 | <0.001 |

Type III ANOVA tests were performed. Total results, including tests found to be not significant, are reported in Table S3. SE, single element gauge axial strains; SE-R, axial strains from the central single element of a rosette gauge; R-pC, principal compressive strains from rosette gauge; R-pT, principal tensile strains from rosette gauge; R-shear, shear strains from rosette gauge.

the rosette gauge, as well as three additional strain magnitudes associated with the rosette gauge (principal tensile, principal compressive and shear). The angle of principal tension to the long

axis of the bone (ϕ_1) was not formally compared across conditions because this angle is included in the calculation of shear strains (Carter, 1978; Biewener and Dial, 1995), and it was deemed

preferable to limit comparisons to variables directly related to strain magnitudes that could be connected to hypotheses about mechanisms of changes in bone shape. Representative strain traces for different substrate conditions are depicted for the femur in Fig. 2, and for the humerus in Fig. 3. The summary and range of all strain metric values recorded can be viewed in Fig. 4. Average stance durations for animals used for femoral strain and humeral strain were 1.04 and 1.22 s, respectively.

General patterns of limb bone strain in iguanas during locomotion

Strain patterns in the iguana femur for FL-LEV surfaces generally match those reported previously (Blob and Biewener, 1999), although our new data include an additional recording location on the ventral aspect of the femur. Longitudinal strains typically increased in absolute magnitude as the foot made contact with the ground, reaching peak values near midstance, though there is some variability across recording locations and substrate types (Fig. 2). For three of the four iguanas from which we collected FL-LEV strains for the femur, strains were tensile on the dorsal surface, and compressive on the anterior surface (Table S1), reflecting loading of the femur in bending with a neutral axis running between these two gauge locations and resembling data collected by Blob and Biewener (1999). Strains on the new, third, ventral location showed low levels of either tensile or compressive strain in the three iguanas with successful recordings, reflecting minor individual variation in loading across the animals. Principal strains for the dorsal recording location were considerably greater in magnitude than longitudinal strains, with magnitudes of ϕ_t at the time of peak strain averaging 49, 57 and 63 deg in the three iguanas with successful femoral rosette recordings. These values of ϕ_t near 45 deg, as well as considerable shear strain magnitudes similar to those of principal strains, reflect the presence of torsional loading in the femur as well as bending during FL-LEV locomotion. Within each animal, strain patterns at a particular location were often consistent across the different locomotor cases; for example, the anterior gauge tended to show compressive strains across all conditions when loads were high (e.g. 40% stance; Fig. 5A). However, loading patterns and magnitudes also varied across other time points and gauge locations (see below).

Strains in the iguana humerus for FL-LEV surfaces were similar among the individual iguanas, but show some differences from comparable humeral measurements reported previously in the American alligator, *Alligator mississippiensis* (Blob et al., 2014). Longitudinal strains increased in absolute magnitude as the manus contacted the ground, reaching single maximum peak values near midstance, though there is some variability across recording locations and substrate types (Fig. 3). For three of the five iguanas from which we collected FL-LEV strains for the humerus, strains were tensile on the posteroventral and ventral surfaces (Table S2). Two of the three animals in which we were able to collect data from the anterior strain gauge indicated compressive strains on that surface, reflecting loading of the humerus in bending with a neutral axis running between the ventral and anterior gauge locations (Fig. 5B). These specific data differ from patterns in *A. mississippiensis* (Blob et al., 2014). Anteriorly placed gauges measured largely compressive strains in iguana humeri, whereas those measured in the alligator humerus were tensile. Similarly, ventrally placed gauges commonly (four out of five individuals) measured tensile strains in iguana humeri (Table S2), and compressive strains in alligators (Blob et al., 2014). Strains on the posteroventral location showed similar tensile measurements as

seen in the ventrally located gauge for most individuals (Table S2). There is not a clear relationship between strain magnitude and gauge location. Principal strain orientations at the time of peak strain (ϕ_t) for the anterior recording location averaged 47 and 53 deg in two iguanas, reflecting torsional loads superimposed on bending in the humerus during FL-LEV locomotion.

Strain magnitude comparisons across substrates

Effects of substrate conditions on strains were limited for the femur. Some strain variables (principal tensile and shear strains, minimum axial strains for the dorsally located gauge in the rosette) showed no effect of substrate on strain magnitude (Table 1). For variables that did show an effect of substrate on load magnitude, including principal compressive strains, maximum axial strains for the dorsal gauge, and strains for the ventral and anterior single element gauges, the angle of the substrate (level versus inclined) had the strongest impact on loads (Table 1). Compliant and curved substrates had effects in only a few cases, and typically only via interactions with either substrate angle or body mass. However, in the cases where substrate angle had a significant effect on strain magnitudes, inclined substrates typically had higher, rather than lower, absolute magnitudes of strain (Table S1). These results are counter to expectations for patterns that would be expected if biomechanical release were a mechanism operating to facilitate morphological diversification in the limb bones of arboreal taxa.

A greater range of significant effects of substrate on strain magnitudes were observed for the humerus (Table 1). Substrate angle had significant effects on several strain variables, though notably less on principal and shear strains than on axial strains. Substrate curvature and compliance had frequent significant effects on load magnitudes as well, though body mass typically only impacts strain magnitudes in interaction with other factors. However, as noted for femoral recordings, there was not a consistent tendency for strains to be reduced among substrates that simulated aspects of arboreal habitats. For many recording locations, absolute strain magnitudes were higher on inclined, compliant or curved substrates in at least some of the animals from which we recorded (Table S2). These results also do not follow patterns expected if biomechanical release were a factor in the morphological diversification of limb bones of arboreal taxa.

Cross-sectional analysis

For the femur, early portions of the stance phase during FL-LEV locomotion showed the neutral axis oriented along a slight anteroventral to posterodorsal axis, with compressive strains on the ventral side of the axis (Fig. 5A). Throughout stance phase, the neutral axis shifted to reflect medial (inward) rotation of the limb. Such shifts in neutral axis orientation during stance are largely similar to patterns observed previously in quadrupedal reptiles using nonparasagittal hindlimb posture (Blob and Biewener, 1999; Butcher et al., 2008; Sheffield et al., 2011). However, on inclined surfaces, more of the cross-section experienced net tension during peak loading than during either condition of level locomotion (flat or compliant). In addition, on the compliant surface, the direction of bending appeared to shift from that during FL-LEV locomotion, with the dorsal aspect loaded in compression, rather than the ventral surface.

For the humerus, during FL-LEV steps, the neutral axis began stance phase oriented along an anteroposterior axis, such that compressive strains were ventral and tensile strains were dorsal (Fig. 5B). Through the course of stance, the neutral axis maintained a fairly consistent orientation for level substrates, but shifted slightly

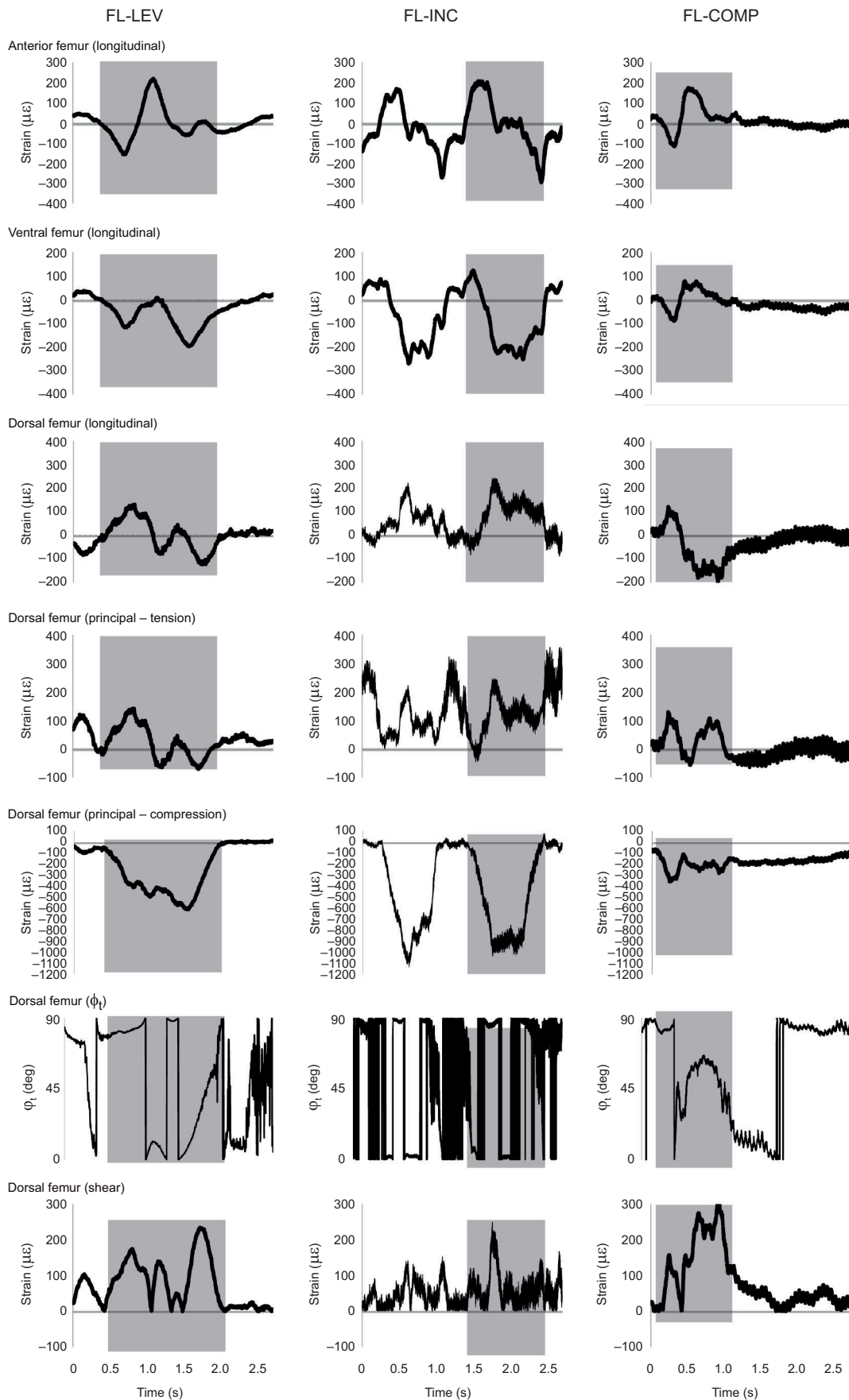


Fig. 2. See next page for legend.

Fig. 2. Femoral strain traces from representative limb cycles comparing flat-level (FL-LEV), flat-incline (FL-INC) and flat-compliant (FL-COMP) surfaces. Shaded regions indicate the time duration in which the pes is in contact with substrate (stance phase) for a single limb cycle. Note that two limb cycles are illustrated for FL-INC traces.

to a more anterodorsal to posteroventral axis for locomotion in other substrates, likely reflecting rotation about the long axis of the bone. Similar to the femur, large portions of the humerus cross-section were loaded in net tension during inclined locomotion, and the orientation of bending shifted during compliant locomotion such that the dorsal aspect of the humerus was in compression and the ventral aspect was in tension.

DISCUSSION

Given our goal of evaluating how features of arboreal habitats influence the loads experienced by limb bones, it is important to acknowledge other factors that have the potential to contribute to variability in strain signals across trials, individuals and species.

For example, differences in gauge placement across individuals have the potential to affect the strain signals recorded. However, in our study, we verified the locations of gauge placements from euthanized specimens after the completion of recordings, confirming that differences in recording locations were minimal. Kinematic differences between individual animals might also contribute to differences in their strain patterns. Although our video records of footfall patterns did not allow us to formally evaluate details of potential kinematic influences on our strain signals, we sought to reduce such possibilities by focusing our comparisons on standard movement behaviors, and none of our individuals exhibited gross abnormalities in their gaits. Kinematic differences between iguanas and other species, even across taxa using non-parasagittal limb posture (Autumn et al., 2006; Zaaf et al., 2001; Irschick and Jayne, 1999), might contribute to differences in observed limb bone strain patterns among lineages, as might differences in limb bone morphology or the insertion of muscles that control the limbs (Blob et al., 2014; Aiello et al., 2013; Reilly and Blob, 2003). Nonetheless, with our efforts to standardize both implantations and experimental conditions, we sought to minimize incidental variation in strain signals in order to concentrate on patterns resulting from our different environmental treatments.

Comparative limb bone loading mechanics during level locomotion

During locomotion on flat-level, non-compliant surfaces, femoral strains recorded from green iguanas in this study were largely consistent with those recorded previously from this species, indicating substantial torsion superimposed on bending (Blob and Biewener, 1999). Torsional loading of the femur appears to be a widespread feature of locomotion among tetrapods using non-parasagittal locomotion (Butcher et al., 2008; Sheffield et al., 2011; Young and Blob, 2015), and potentially among species using more upright posture as well (Carrano, 1998; Butcher et al., 2011; Copploe et al., 2015). Femoral bending is also common among non-parasagittal taxa, exhibiting a range of patterns. Limited recording locations for the femur had not allowed cross-sectional analyses of strains in the previous study of iguana limb loading (Blob and Biewener, 1999). However, the bending orientation and load distribution identified in this study generally resembled those for the femur of tegu lizards (Sheffield et al., 2011) and turtles (Butcher et al., 2008), with an anterior to posterior orientation of the neutral axis and compressive strains on the ventral aspect of the femur

during peak loading (40% stance) on level surfaces (Fig. 5A). In contrast, though the inclination of the neutral axis is generally similar in alligators the direction of bending appears to be opposite, with compressive strains on the dorsal aspect of the femur (Blob and Biewener, 1999).

Similarities in torsion and the plane of femoral bending across these taxa likely reflect at least general similarities in their limb kinematics, particularly the extent to which the femur rotates about its long axis. Long axis rotation of limb bones changes the orientation of anatomical surfaces with respect to absolute space, such that the bone cross-section could be envisioned as rotating through an essentially horizontal plane of bending imposed on the bone by largely vertical ground reaction forces (Blob and Biewener, 2001; Kawano and Blob, 2013; Kawano et al., 2016). This possibility could be tested through the use of experimental techniques such as X-ray Reconstruction of Moving Morphology (XROMM; Brainerd et al., 2010), which can be particularly effective at resolving axial rotation of limb skeletal elements (Kambic et al., 2014; Mayerl et al., 2016). In contrast, differences in the orientation of bending (i.e. differences in which femoral surfaces are exposed to compression versus tension) may relate to differences in the activity patterns of the muscles powering hindlimb steps across these species. Simultaneous measurements of bone strains and muscle activity and shortening in the hindlimbs of turtles have indicated that changes in the direction of femoral bending through the course of stance can relate to changes in the relative activity and shortening of ventrally situated hip retractor muscles, such as *M. flexor tibialis internus*, and dorsally situated knee extensors, such as *M. femorotibialis* (Aiello et al., 2013). Although data on muscle activity patterns indicate similar onset and offset times for these muscles between turtles (Aiello et al., 2013) and alligators (Gatesy, 1997; Reilly and Blob, 2003), simultaneous measurements of muscle shortening that could give insight into the relative intensity of their contractions are not available for alligators, nor are comparable data on muscle function available for either iguanas or tegus. In this context, further data on the timing and intensity of shortening between major groups of thigh muscles across these taxa could help to explain why bending places the ventral aspect of the femur in compression in some non-parasagittal taxa, but in tension in others.

Our recordings from the iguana humerus are the first humeral strains recorded from any lepidosaur. Strain patterns were different from those of the femur in some respects, despite both elements being proximal limb bones. For example, although torsion was prominent in the humerus as it was in the femur, the orientation of bending differed between these bones, placing the dorsal surface of the femur in tension in iguanas, but the ventral and posteroventral surfaces in tension in the humerus (Fig. 5B). Contrasts in loading between the femur and humerus were also observed in sprawling salamanders, and were interpreted as differences in the initial orientation and axial rotations of these elements through stance (Kawano et al., 2016). However, in addition to differences in axial rotation between these elements, it is also possible that the humerus and femur of iguanas differ in the magnitude of axial compression that is superimposed on their cross-sections in support of body weight. Increases and reductions of axial compression can shift the neutral axis of bending away from the cross-sectional centroids of bones, leading to changes in the distribution of tension and compression about the cortex (Blob and Biewener, 1999). Because the iguana forelimb is smaller than the hindlimb, ground reaction force magnitudes (or the severity of their effect) may differ between the humerus and femur, contributing to differences in the distribution of their strains. Iguana humeral strains also differ somewhat from those of American alligators, which exhibit tensile

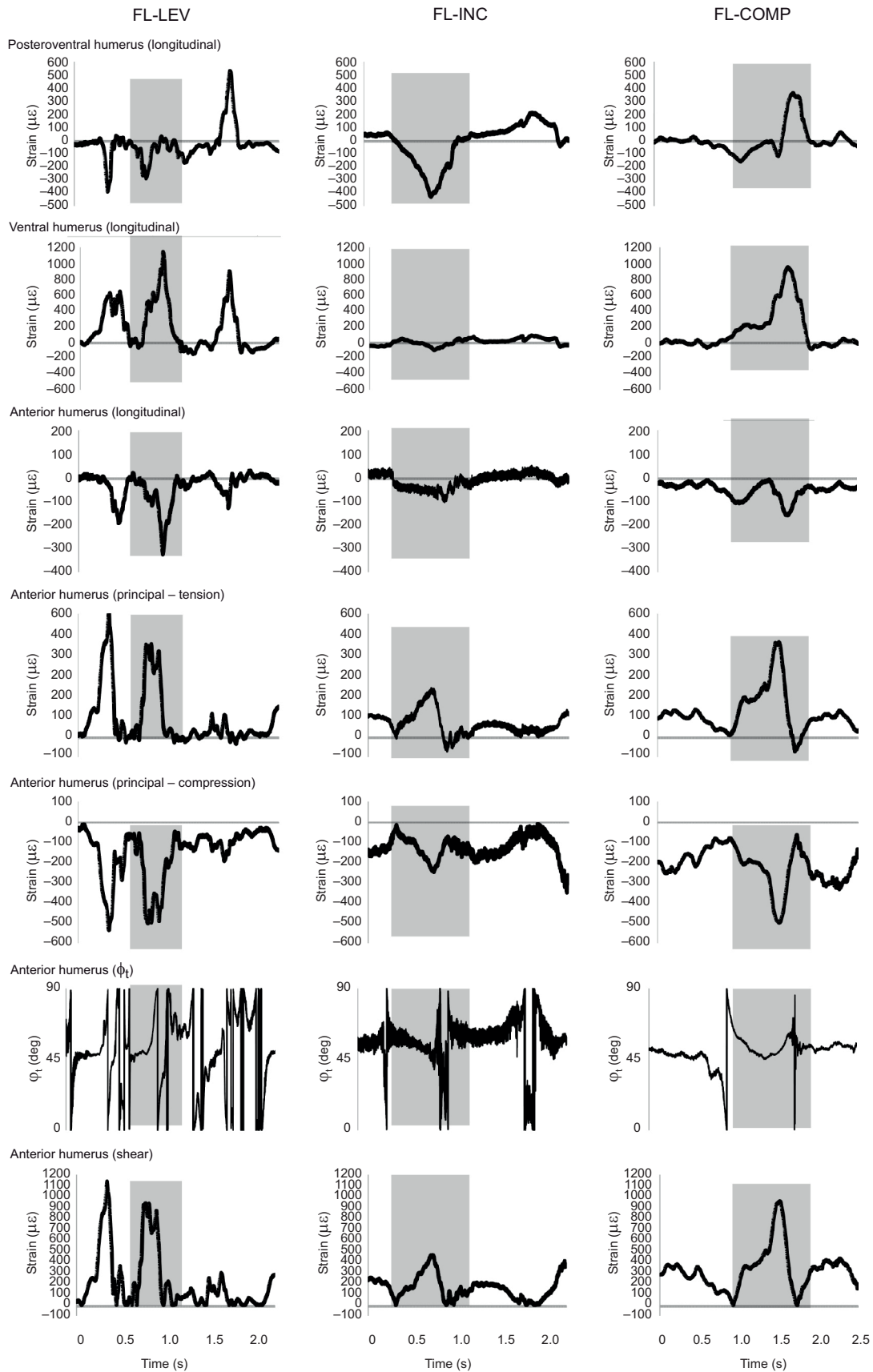


Fig. 3. Humeral strain traces from representative limb cycles comparing flat-level (FL-LEV), flat-inclined (FL-INC) and flat-compliant (FL-COMP) surfaces. Shaded regions indicate the time duration in which the manus is in contact with substrate (stance phase) for a single limb cycle. Note that multiple limb cycles are illustrated for FL-LEV traces.

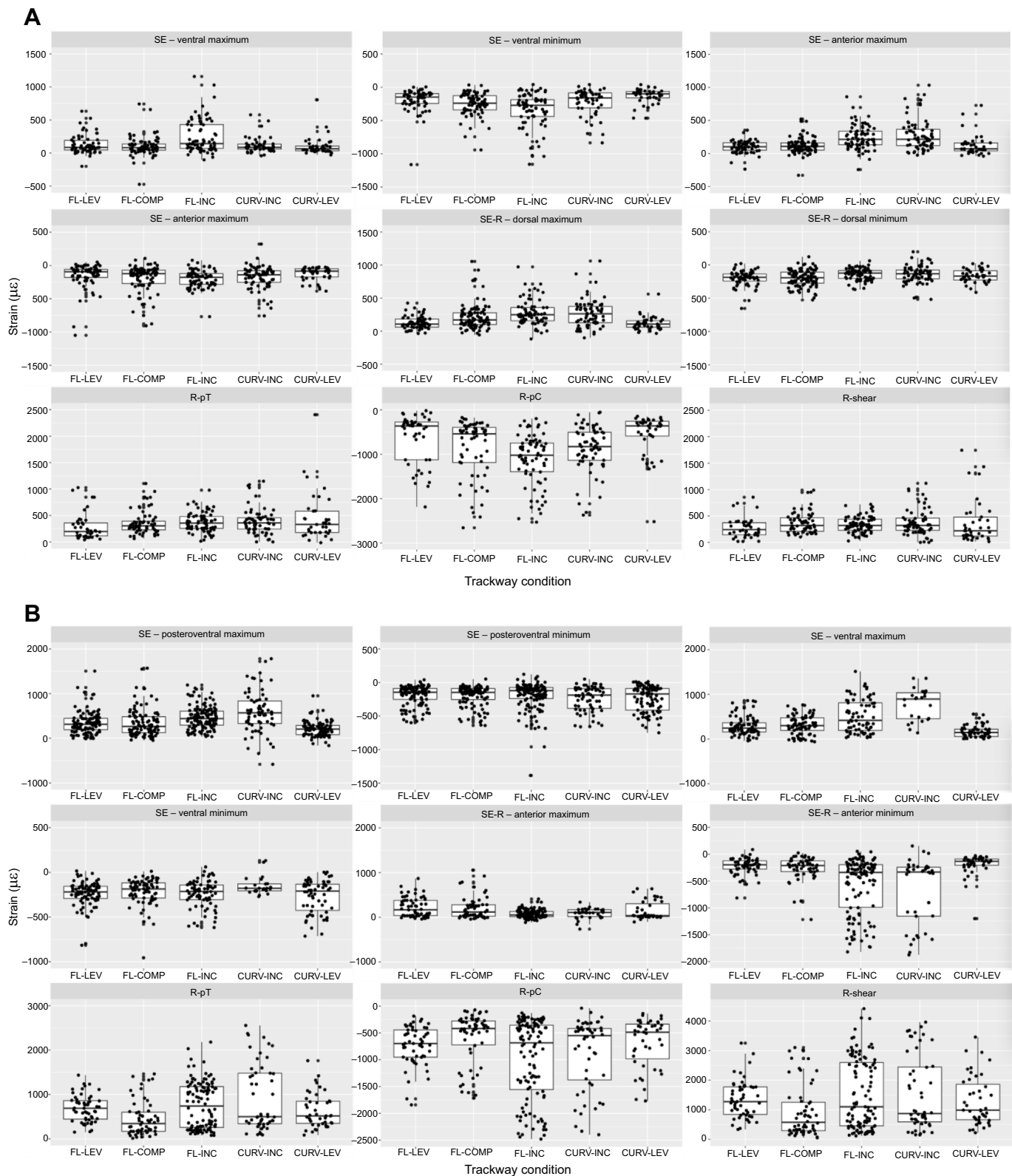
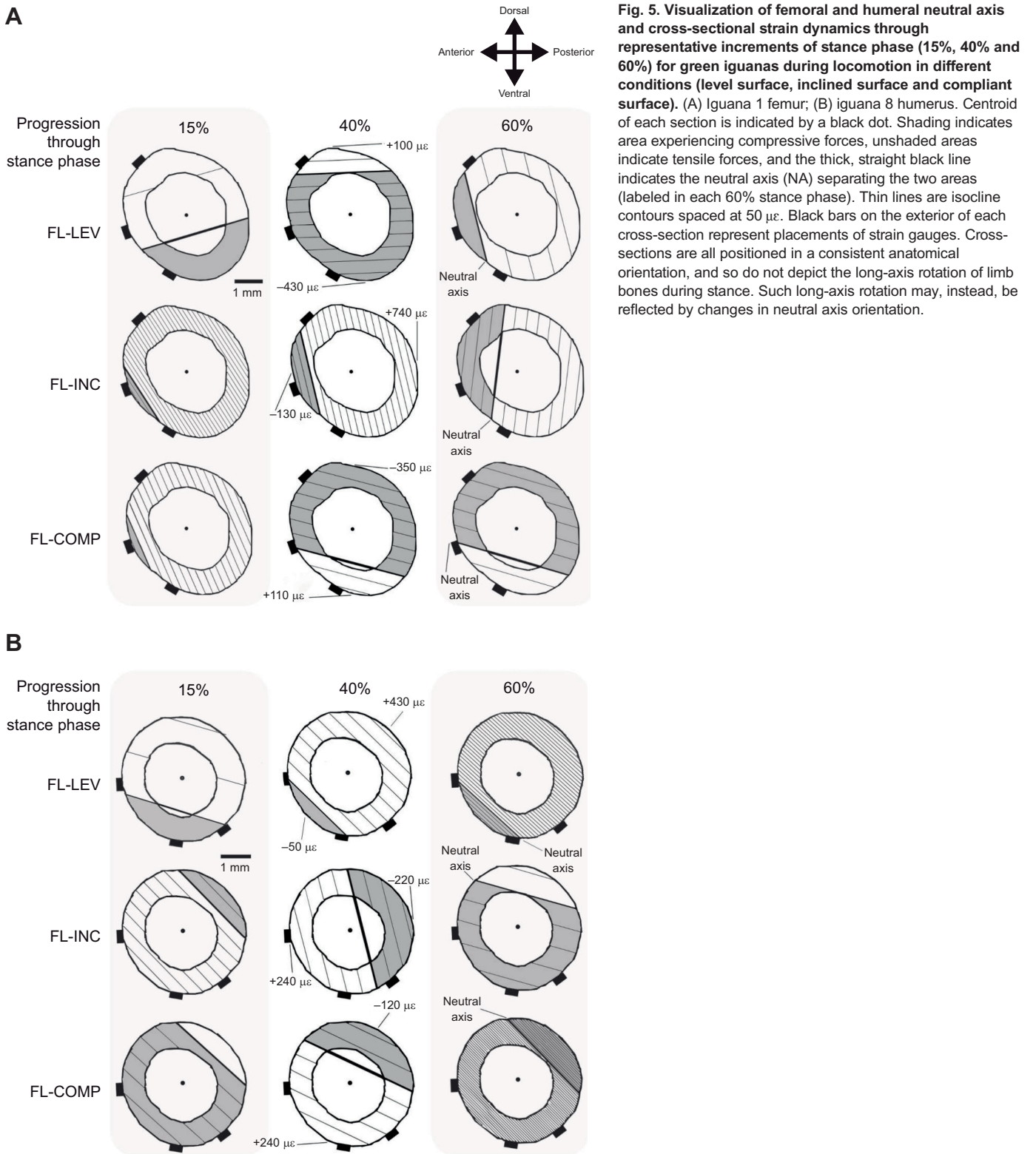


Fig. 4. Jitter-box plots detailing summary values and strain metric ranges measured across individuals. (A) Hindlimb; (B) forelimb. SE, single element gauge axial strains; SE-R, axial strains from the central single element of a rosette gauge; R-pC, principal compressive strains from rosette gauge; R-pT, principal tensile strains from rosette gauge; R-shear, shear strains from rosette gauge.

strains extending to the anterior and anteroventral surfaces during bending (Blob et al., 2014). Although the factors that contribute to differences in the distributions of humeral strains between iguanas and

alligators remain unclear, differences in the extent of axial compression does not seem a very likely explanation because the forelimbs are similar in proportion to the body in both taxa.



Environmental effects on limb bone loading and implications for biomechanical release

Out of all the simulated environmental conditions that we compared, surface incline had the most appreciable effects on femoral loads during locomotion, though other substrate conditions did appear to influence humeral loads to a greater degree (Table 1). These results indicate that all of the distinctive components of arboreal habitats

(e.g. incline, compliance and curvature) could have some influence on the loads that limb bones experience, though effects of incline may be the most widespread (Table 1).

Data from this study were collected with the goal of gaining insight into how the limbs of arboreal taxa lengthened through evolutionary time. In particular, might arboreal locomotion have provided a release from the biomechanical loads typical of terrestrial locomotion and,

thereby, provided an opportunity for morphological change? Our results do not support this conclusion. Rather than showing lower loads during simulations of arboreal conditions, iguana limb bones frequently showed elevated absolute magnitudes of femoral strains in response to substrate inclination, as well as elevated humeral strain magnitudes in response to compliant and curved surfaces. Surface reaction forces from vertically climbing geckos may give some insight into these effects, as the overturning moment indicated in geckos might lead to increases in compression for the hindlimb bones (Autumn et al., 2006). However, loading changes related to curved and compliant substrates, as well as those for the forelimb, may not be explained by toppling moments and might, instead, be due to changes in factors such as muscle activation under novel locomotor conditions (Higham and Jayne, 2004; Aiello et al., 2013). Nonetheless, our results indicate that the evolution of longer limb bones in arboreal species may actually have occurred in spite of increases in overall strain, rather than having been facilitated by a reduction in loads. For example, our analyses of planar strain distributions in two of our experimental iguanas allowed calculations of potential maximum femoral strains during inclined locomotion, giving values of 3062 ± 1251 and $4164 \pm 138 \mu\epsilon$. Compared with the published yield strain value of $9819 \pm 611 \mu\epsilon$ for the iguana femur (Blob and Biewener, 1999), such strains would reflect a safety factor of between 2.4 and 3.2 – a sizeable margin of safety, but much less than published estimates of 10.8 for the iguana femur during locomotion on level ground (Blob and Biewener, 1999). Biomechanical release was likely an influential mechanism in other evolutionary habitat transitions, such as the secondary invasion of aquatic habitats by tetrapods (Young and Blob, 2015; Young et al., 2017). However, it seems unlikely to have contributed to morphological changes across terrestrial-to-arboreal habitat transitions, suggesting that limb elongation in these transitions was driven by functional demands or other factors that superseded any potential costs of higher limb bone loads.

Acknowledgements

We thank J. Wyneken, K. Gilroy, V. Kolehmainen, C. Kolehmainen, C. Kolehmainen, M. Bennett and S. Diamond for assistance with collecting iguanas. We also thank C. Mayerl, A. Palecek, C. Kinsey, N. Schneider, A. McKamy and A. Riley for assistance with experiments, and B. Hedrick, J. Sanchez and E. Prior for guidance and discussion. Results and Discussion in this paper are reproduced from the MSc thesis of V. David Munteanu (Clemson University, 2020).

Competing interests

The authors declare no competing or financial interests.

Author contributions

Conceptualization: V.D.M., R.W.B.; Methodology: V.D.M., K.M.D., R.W.B.; Software: V.M.D., K.M.D., R.W.B.; Validation: V.D.M., R.W.B.; Formal analysis: V.D.M., K.M.D.; Investigation: V.D.M., K.M.D., R.W.B.; Resources: V.D.M., K.M.D., R.W.B.; Writing - original draft: V.D.M., V.D.M., R.W.B.; Writing - review & editing: V.D.M., K.M.D., R.W.B.; Visualization: V.D.M.; Supervision: R.W.B.; Project administration: R.W.B.; Funding acquisition: V.D.M., R.W.B.

Funding

This work was supported by a Society for Integrative and Comparative Biology Grant-in Aid-of-Research (V.D.M.) and Clemson University Creative Inquiry Project 479 (R.W.B.). Open access funding provided by Clemson University. Deposited in PMC for immediate release.

Data availability

Data upon which analyses are based are available from the figshare repository: <https://doi.org/10.6084/m9.figshare.c.6252393.v1>.

ECR Spotlight

This article has an associated ECR Spotlight interview with V. David Munteanu.

References

- Aiello, B. R., Blob, R. W. and Butcher, M. T.** (2013). Correlation of muscle function and bone strain in the hindlimb of the river cooter turtle (*Pseudemys concinna*). *J. Morphol.* **274**, 1060-1069. doi:10.1002/jmor.20162
- Aiello, B. R., Westneat, M. W. and Hale, M. E.** (2017). Mechanosensation is evolutionarily tuned to locomotor mechanics. *Proc. Natl. Acad. Sci. USA* **114**, 4459-4464. doi:10.1073/pnas.1616839114
- Autumn, K., Hsieh, T. S., Dudek, D. M., Chen, J., Chitaphan, C. and Full, R. J.** (2006). Dynamics of geckos running vertically. *J. Exp. Biol.* **209**, 260-272. doi:10.1242/jeb.01980
- Biewener, A. A.** (1983). Allometry of quadrupedal locomotion: the scaling of duty factor, bone curvature and limb orientation to body size. *J. Exp. Biol.* **105**, 147-171. doi:10.1242/jeb.105.1.147
- Biewener, A. A.** (1990). Biomechanics of mammalian terrestrial locomotion. *Science* **250**, 1097-1103. doi:10.1126/science.2251499
- Biewener, A. A. and Dial, K. P.** (1995). *In-vivo* strain in the humerus of pigeons (*Columba livia*) during flight. *J. Morphol.* **225**, 61-75. doi:10.1002/jmor.1052250106
- Blob, R. W. and Biewener, A. A.** (1999). *In vivo* locomotor strain in the hindlimb bones of *Alligator mississippiensis* and *Iguana iguana*: implications for the evolution of limb bone safety factor and non-sprawling limb posture. *J. Exp. Biol.* **202**, 1023-1046. doi:10.1242/jeb.202.9.1023
- Blob, R. W. and Biewener, A. A.** (2001). Mechanics of limb bone loading during terrestrial locomotion in the green iguana (*Iguana iguana*) and American alligator (*Alligator mississippiensis*). *J. Exp. Biol.* **204**, 1099-1122. doi:10.1242/jeb.204.6.1099
- Blob, R. W., Espinoza, N. R., Butcher, M. T., Lee, A. H., D'amico, A. R., Baig, F. and Sheffield, K. M.** (2014). Diversity of limb-bone safety factors for locomotion in terrestrial vertebrates: evolution and mixed chains. *Int. Comp. Biol.* **54**, 1058-1071. doi:10.1093/icb/ucu032
- Brainerd, E. L., Baier, D. B., Gatesy, S. M., Hedrick, T. L., Metzger, K. A., Gilbert, S. L. and Crisco, J. J.** (2010). X-ray Reconstruction of Moving Morphology (XROMM): precision, accuracy and applications in comparative biomechanics research. *J. Exp. Zool. A* **313**, 262-279. doi:10.1002/jez.589
- Butcher, M. T., Espinoza, N. R., Cirilo, S. R. and Blob, R. W.** (2008). *In vivo* strains in the femur of river cooter turtles (*Pseudemys concinna*) during terrestrial locomotion: tests of force-platform models of loading mechanics. *J. Exp. Biol.* **211**, 2397-2407. doi:10.1242/jeb.018986
- Butcher, M. T., White, B. J., Hudzik, N. B., Gosnell, W. C., Parrish, J. H. and Blob, R. W.** (2011). *In vivo* strains in the femur of the Virginia opossum (*Didelphis virginiana*) during terrestrial locomotion: testing hypotheses of evolutionary shifts in mammalian bone loading and design. *J. Exp. Biol.* **214**, 2631-2640. doi:10.1242/jeb.049544
- Byron, C., Kunz, H., Matuszek, H., Lewis, S. and Van Valkinburgh, D.** (2011). Rudimentary pedal grasping in mice and implications for terminal branch arboreal quadrupedalism. *J. Morphol.* **272**, 230-240. doi:10.1002/jmor.10909
- Calbet, J. A., Moysi, J. S., Dorado, C. and Rodriguez, L. P.** (1998). Bone mineral content and density in professional tennis players. *Calcif. Tissue Int.* **62**, 491-496.
- Carlson, K. J. and Judex, S.** (2007). Increased non-linear locomotion alters diaphyseal bone shape. *J. Exp. Biol.* **210**, 3117-3125. doi:10.1242/jeb.006544
- Carrano, M. T.** (1998). Locomotion in non-avian dinosaurs: integrating data from hindlimb kinematics, *in vivo* strains, and bone morphology. *Paleobiology* **24**, 450-469. doi:10.1017/S0094837300020108
- Carter, D. R.** (1978). Anisotropic analysis of strain rosette information from cortical bone. *J. Biomech.* **11**, 199-202. doi:10.1016/0021-9290(78)90013-1
- Cartmill, M.** (1985). Climbing. In *Functional Vertebrate Morphology* (ed. M. B. Hildebrand, K. F. Liem and D. M. Wake), pp. 73-88. Cambridge, MA: Belknap Press.
- Copploe, J. V., Blob, R. W., Parrish, J. H. and Butcher, M. T.** (2015). *In vivo* strains in the femur of the nine-banded armadillo (*Dasypus novemcinctus*). *J. Morphol.* **276**, 889-899. doi:10.1002/jmor.20387
- Dally, J. W. and Riley, W. F.** (1991). *Experimental Stress Analysis*. New York: McGraw-Hill.
- Demes, B. and Carlson, K. J.** (2009). Locomotor variation and bending regimes of capuchin limb bones. *Am. J. Phys. Anthropol.* **139**, 558-571. doi:10.1002/ajpa.21020
- Gatesy, S. M.** (1997). An electromyographic analysis of hindlimb function in *Alligator* during terrestrial locomotion. *J. Morphol.* **234**, 197-212. doi:10.1002/(SICI)1097-4687(199711)234:2<197::AID-JMOR6>3.0.CO;2-9
- Granatosky, M. C., Fitzsimons, A., Zeining, A. and Schmitt, D.** (2018). Mechanisms for the functional differentiation of the propulsive and braking roles of the forelimbs and hindlimbs during quadrupedal walking in primates and felines. *J. Exp. Biol.* **221**, jeb162917. doi:10.1242/jeb.162917
- Hatfield, J. W.** (1996). *Green Iguana: The Ultimate Owner's Manual*. Portland, OR: Dunthorpe Press.
- Herrel, A., Tolley, K. A., Measey, G. J., Da Silva, J. M., Potgieter, D. F., Boller, E., Boistel, R. and Vanhooydonck, B.** (2013). Slow but tenacious: an analysis of running and gripping performance in chameleons. *J. Exp. Biol.* **216**, 1025-1030. doi:10.1242/jeb.078618

- Higham, T. E. and Jayne, B. C.** (2004). *In vivo* muscle activity in the hindlimb of the arboreal lizard, *Chamaeleo calyptrotus*: general patterns and the effects of incline. *J. Exp. Biol.* **207**, 249-261. doi:10.1242/jeb.00745
- Iriarte-Díaz, J.** (2002). Differential scaling of locomotor performance in small and large terrestrial mammals. *J. Exp. Biol.* **205**, 2897-2908. doi:10.1242/jeb.205.18.2897
- Irschick, D. J. and Jayne, B. C.** (1999). Comparative three-dimensional kinematics of the hindlimb for high-speed bipedal and quadrupedal locomotion of lizards. *J. Exp. Biol.* **202**, 1047-1065. doi:10.1242/jeb.202.9.1047
- Ito, I. H., Mantovani, A. M., Agostineti, R. R., Costa Junior, P., Zanuto, E. F., Christofaro, D. G., Ribeiro, L. P. and Fernandes, R. A.** (2016). Practice of martial arts and bone mineral density in adolescents of both sexes. *Rev. Paul. Pediatr.* **34**, 210-215. doi:10.1016/j.rpped.2015.09.001
- Kambic, R. E., Roberts, T. J. and Gatesy, S. M.** (2014). Long-axis rotation: a missing degree of freedom in avian bipedal locomotion. *J. Exp. Biol.* **217**, 2770-2782. doi:10.1242/jeb.101428
- Kawano, S. M. and Blob, R. W.** (2013). Propulsive forces of mudskipper fins and salamander limbs during terrestrial locomotion: implications for the invasion of land. *Int. Comp. Biol.* **53**, 283-294. doi:10.1093/icb/ict051
- Kawano, S. M., Economy, D. R., Kennedy, M. S., Dean, D. and Blob, R. W.** (2016). Comparative limb bone loading in the humerus and femur of the tiger salamander: testing the 'mixed-chain' hypothesis for skeletal safety factors. *J. Exp. Biol.* **219**, 341-353. doi:10.1242/jeb.125799
- Kemp, T. J., Bachus, K. N., Nairn, J. A. and Carrier, D. R.** (2005). Functional trade-offs in the limb bones of dogs selected for running versus fighting. *J. Exp. Biol.* **208**, 3475-3482. doi:10.1242/jeb.01814
- Kilbourne, B. M. and Hoffman, L. C.** (2015). Energetic benefits and adaptations in mammalian limbs: scale effects and selective pressures. *Evolution* **69**, 1546-1559. doi:10.1111/evo.12675
- Lammers, A. R. and Gauntner, T.** (2008). Mechanics of torque generation during quadrupedal arboreal locomotion. *J. Biomech.* **41**, 2388-2395. doi:10.1016/j.jbiomech.2008.05.038
- Lieberman, D. E., Polk, J. D. and Demes, B.** (2004). Predicting long bone loading from cross-sectional geometry. *Am. J. Phys. Anthropol.* **123**, 156-171. doi:10.1002/ajpa.10316
- Maie, T., Schoenfuss, H. L. and Blob, R. W.** (2012). Performance and scaling of a novel locomotor structure: adhesive capacity of climbing gobiid fishes. *J. Exp. Biol.* **215**, 3925-3936. doi:10.1242/jeb.072967
- Mayerl, C. J., Brainerd, E. L. and Blob, R. W.** (2016). Pelvic girdle mobility of cryptodire and pleurodire turtles during walking and swimming. *J. Exp. Biol.* **219**, 2650-2658. doi:10.1242/jeb.141622
- Mchenry, C. R., Clausen, P. D., Daniel, W. J., Meers, M. B. and Pendharkar, A.** (2006). Biomechanics of the rostrum in crocodylians: a comparative analysis using finite-element modeling. *Anat. Rec.* **288**, 827-849. doi:10.1002/ar.a.20360
- Meldrum, D. J., Dagosto, M. and White, J.** (1997). Hindlimb suspension and hind foot reversal in *Varecia variegata* and other arboreal mammals. *Am. J. Phys. Anthropol.* **103**, 85-102. doi:10.1002/(SICI)1096-8644(199705)103:1<85::AID-AJPA6>3.0.CO;2-C
- Reilly, S. M. and Blob, R. W.** (2003). Motor control of locomotor hindlimb posture in the American alligator (*Alligator mississippiensis*). *J. Exp. Biol.* **206**, 4327-4340. doi:10.1242/jeb.00688
- Rivera, G. and Stayton, C. T.** (2011). Finite element modeling of shell shape in the freshwater turtle *Pseudemys concinna* reveals a trade-off between mechanical strength and hydrodynamic efficiency. *J. Morphol.* **272**, 1192-1203. doi:10.1002/jmor.10974
- Romer, A. S.** (1922). The locomotor apparatus of certain primitive and mammal-like reptiles. *Bull. Am. Mus. Nat. Hist.* **46**, 517-606.
- Rooney, L.** (2018). Postcranial morphology and the locomotor adaptations of extant and extinct crocodylomorphs and lepidosaurs. MSc thesis, *East Tennessee State University*.
- Sheffield, K. M., Butcher, M. T., Shugart, S. K., Gander, J. C. and Blob, R. W.** (2011). Locomotor loading mechanics in the hindlimbs of tegu lizards (*Tupinambis merianae*): comparative and evolutionary implications. *J. Exp. Biol.* **214**, 2616-2630. doi:10.1242/jeb.048801
- Swartz, S. M., Bertram, J. and Biewener, A. A.** (1989). Telemetered *in vivo* strain analysis of locomotor mechanics of brachiating gibbons. *Nature* **342**, 270-272. doi:10.1038/342270a0
- Turner, C. H. and Pavalko, F. M.** (1998). Mechanotransduction and functional response of the skeleton to physical stress: the mechanisms and mechanics of bone adaptation. *J. Orthop. Sci.* **3**, 346-355. doi:10.1007/s007760050064
- Wainwright, P. C., Alfaro, M. E., Bolnick, D. I. and Hulsey, C. D.** (2005). Many-to-one mapping of form to function: a general principle in organismal design? *iCB* **45**, 256-262. doi:10.1093/icb/45.2.256
- Young, V. K. H. and Blob, R. W.** (2015). Limb bone loading in swimming turtles: changes in loading facilitate transitions from tubular to flipper-shaped limbs during aquatic invasions. *Biol. Lett.* **11**, 20150110. doi:10.1098/rsbl.2015.0110
- Young, V. K. H., Wienands, C. E., Wilburn, B. P. and Blob, R. W.** (2017). Humeral loads during swimming and walking in turtles: implications for morphological change during aquatic reinvasions. *J. Exp. Biol.* **220**, 3873-3877. doi:10.1242/jeb.156836
- Zaaf, A., Herrel, A., Aerts, P. and De Vree, F.** (1999). Morphology and morphometrics of the appendicular musculature in geckoes with different locomotor habits (Lepidosauria). *Zoomorphology* **119**, 9-22.

Table S1. Hindlimb strain data across strain gauge metrics, reported for each individual from which data were successfully collected, with mass and snout-vent length (SVL).

“R” in gauge metric row indicates that this metric was associated with the rosette gauge. Values in first five rows indicate the average maximum/minimum strain (units in microstrain, $\mu\epsilon = 10^{-6} \times$ strain) \pm standard deviation, with number of steps in parentheses.

| Animal | Gauge metric | FL-LEV | FL-COMP | FL-INC | CURV-INC | CURV-LEV |
|-----------------------------------|--------------------------|-------------------------|-------------------------|--------------------------|--------------------------|-------------------------|
| IG01 - mass=1.27 kg; SVL=34.29 cm | SE-Ventral | -164 \pm 156 (N = 13) | -78 \pm 57 (N = 23) | -108 \pm 66 (N = 13) | -73 \pm 63 (N = 13) | -117 \pm 79 (N = 8) |
| | SE-Anterior | -208 \pm 125 (N = 13) | -297 \pm 198 (N = 23) | -758 \pm 239 (N = 13) | -336 \pm 304 (N = 13) | -117 \pm 98 (N = 8) |
| | SE-R Dorsal | 119 \pm 61 (N = 13) | 191 \pm 103 (N = 23) | 570 \pm 189 (N = 13) | 426 \pm 344 (N = 13) | 108 \pm 80 (N = 8) |
| | R-pT | 443 \pm 303 (N = 13) | 351 \pm 187 (N = 23) | 576 \pm 187 (N = 13) | 475 \pm 291 (N = 13) | 417 \pm 180 (N = 8) |
| | R-pC | -416 \pm 259 (N = 13) | -600 \pm 380 (N = 23) | -1680 \pm 509 (N = 13) | -984 \pm 832 (N = 11) | -322 \pm 152 (N = 8) |
| | R-Shear | 278 \pm 155 (N = 13) | 281 \pm 142 (N = 23) | 489 \pm 104 (N = 13) | 416 \pm 384 (N = 13) | 111 \pm 41 (N = 8) |
| | R-Phi (units in degrees) | 49 \pm 26 (N = 13) | 45 \pm 27 (N = 23) | 22 \pm 20 (N = 13) | 43 \pm 32 (N = 13) | 39 \pm 38 (N = 8) |
| IG02 - mass=1.05 kg; SVL=33.66 | SE-Ventral | 133 \pm 76 (N = 25) | 172 \pm 119 (N = 19) | 161 \pm 97 (N = 21) | 177 \pm 87 (N = 19) | 159 \pm 50 (N = 22) |
| | SE-Anterior | -115 \pm 92 (N = 25) | -185 \pm 171 (N = 19) | -334 \pm 160 (N = 21) | -236 \pm 122 (N = 19) | -106 \pm 87 (N = 22) |
| | SE-R Dorsal | 113 \pm 88 (N = 25) | 173 \pm 130 (N = 19) | 274 \pm 112 (N = 21) | 276 \pm 121 (N = 19) | 143 \pm 110 (N = 22) |
| | R-pT | 158 \pm 87 (N = 25) | 274 \pm 158 (N = 19) | 316 \pm 114 (N = 21) | 325 \pm 124 (N = 19) | 600 \pm 566 (N = 20) |
| | R-pC | -435 \pm 417 (N = 25) | -797 \pm 490 (N = 18) | -1400 \pm 557 (N = 20) | -1090 \pm 493 (N = 19) | -671 \pm 568 (N = 22) |
| | R-Shear | 260 \pm 186 (N = 25) | 378 \pm 123 (N = 19) | 324 \pm 144 (N = 21) | 376 \pm 144 (N = 19) | 614 \pm 468 (N = 20) |
| | R-Phi (units in degrees) | 63 \pm 40 (N = 25) | 53 \pm 25 (N = 19) | 69 \pm 28 (N = 21) | 76 \pm 12 (N = 19) | 47 \pm 24 (N = 20) |

| Animal | Gauge metric | FL-LEV | FL-COMP | FL-INC | CURV-INC | CURV-LEV |
|-----------------------------------|--------------------------|-------------------|-------------------|-------------------|-------------------|-------------------|
| IG03 - mass=0.86 kg; SVL=30.8 cm | SE-Ventral | 78±91 (N = 27) | 114±131 (N = 32) | 353±206 (N = 24) | 328±218 (N = 22) | 114±204 (N = 12) |
| | SE-Anterior | -258±219 (N = 24) | -251±148 (N = 32) | -269±120 (N = 24) | -297±132 (N = 4) | -190±144 (N = 12) |
| | SE-R Dorsal | -197±83 (N = 27) | -132±78 (N = 32) | -165±90 (N = 24) | -181±75 (N = 18) | -209±99 (N = 12) |
| | R-pT | 845±1 (N = 2) | | 313±177 (N = 24) | 281±207 (N = 17) | 157±142 (N = 9) |
| | R-pC | -1543±331 (N = 7) | | -802±429 (N = 24) | -630±368 (N = 17) | -459±327 (N = 9) |
| | R-Shear | | | 283±158 (N = 24) | 345±256 (N = 17) | 139±140 (N = 9) |
| | R-Phi (units in degrees) | | | 48±25 (N = 24) | 31±21 (N = 17) | |
| IG04 - mass=0.86 kg; SVL=30.16 cm | SE-Ventral | | | 304±181 (N = 17) | 462±244 (N = 18) | |
| | SE-Anterior | | | 285±322 (N = 16) | 125±49 (N = 15) | |
| | SE-R Dorsal | | | 256±94 (N = 17) | 333±66 (N = 18) | |
| | R-pT | | | 354±650 (N = 17) | 487±287 (N = 18) | |
| | R-pC | | | -768±238 (N = 17) | -809±264 (N = 18) | |
| | R-Shear | | | 297±663 (N = 17) | 391±192 (N = 18) | |
| | R-Phi (units in degrees) | | | 16±13 (N = 17) | 18±18 (N = 18) | |

| Animal | Gauge metric | FL-LEV | FL-COMP | FL-INC | CURV-INC | CURV-LEV |
|-----------------------------------|--------------------------|-------------------|--------------------|--------|----------|----------|
| IG05 - mass=1.05 kg; SVL=36.51 cm | SE-Ventral | | | | | |
| | SE-Anterior | -630±594 (N = 2) | -529±220 (N = 15) | | | |
| | SE-R Dorsal | 268±38 (N = 2) | 451±307 (N = 15) | | | |
| | R-pT | 326±120 (N = 2) | 531±281 (N = 15) | | | |
| | R-pC | -1392±376 (N = 2) | -1782±570 (N = 13) | | | |
| | R-Shear | 589±377 (N = 2) | 563±248 (N = 15) | | | |
| | R-Phi (units in degrees) | 57±38 (N = 2) | 52±31 (N = 15) | | | |

Table S2. Forelimb strain data across strain gauge metrics reported for each individual from which data were successfully collected, with mass and snout-vent length (SVL). “R” in gauge metric row indicates that this metric was associated with the rosette gauge. Values in first five rows indicate the average maximum/minimum strain (units in microstrain, $\mu\epsilon = 10^{-6} \times \text{strain}$) \pm standard deviation, with number of steps in parentheses.

| Animal | Gauge metric | FL-LEV | FL-COMP | FL-INC | CURV-INC | CURV-LEV |
|-----------------------------------|--------------------------|-------------------------|-------------------------|--------------------------|--------------------------|-------------------------|
| IG07 - mass=1.18 kg; SVL=29.72 cm | SE-Postero-ventral | 266 \pm 149 (N = 23) | 241 \pm 113 (N = 14) | 430 \pm 143 (N = 34) | 478 \pm 153 (N = 16) | |
| | SE-Ventral | 430 \pm 244 (N = 23) | 478 \pm 200 (N = 19) | 833 \pm 274 (N = 34) | 977 \pm 222 (N = 16) | |
| | SE-R Anterior | | | -1338 \pm 262 (N = 34) | -1329 \pm 408 (N = 16) | |
| | R-pT | | | | | |
| | R-pC | | | | | |
| | R-Shear | | | | | |
| | R-Phi (units in degrees) | | | | | |
| IG08 - mass=2.05 kg; 32.39 cm | SE-Postero-ventral | 647 \pm 309 (N = 23) | 531 \pm 448 (N = 25) | 178 \pm 118 (N = 18) | | 248 \pm 128 (N = 26) |
| | SE-Ventral | 213 \pm 216 (N = 23) | 157 \pm 174 (N = 25) | 139 \pm 82 (N = 18) | | 85 \pm 80 (N = 26) |
| | SE-R Anterior | -136 \pm 81 (N = 23) | -141 \pm 110 (N = 25) | -104 \pm 45 (N = 18) | | -132 \pm 58 (N = 26) |
| | R-pT | 434 \pm 176 (N = 23) | 333 \pm 178 (N = 25) | 271 \pm 90 (N = 18) | | 374 \pm 140 (N = 26) |
| | R-pC | -420 \pm 145 (N = 23) | -386 \pm 137 (N = 25) | -297 \pm 65 (N = 18) | | -371 \pm 130 (N = 26) |
| | R-Shear | 739 \pm 413 (N = 23) | 683 \pm 309 (N = 25) | 528 \pm 167 (N = 18) | | 719 \pm 267 (N = 26) |
| | R-Phi (units in degrees) | 47 \pm 9 (N = 23) | 49 \pm 4 (N = 25) | 50 \pm 4 (N = 18) | | 50 \pm 3 (N = 26) |

| Animal | Gauge metric | FL-LEV | FL-COMP | FL-INC | CURV-INC | CURV-LEV |
|--------------------------------|--------------------------|-------------------|-------------------|-------------------|-------------------|-------------------|
| IG09 - mass=1.22 kg; SVL=35.81 | SE-Postero-ventral | | | 178±154 (N = 23) | 253±406 (N = 22) | |
| | SE-Ventral | | | | | |
| | SE-R Anterior | | | -329±116 (N = 23) | -224±137 (N = 22) | |
| | R-pT | | | 651±296 (N = 23) | 413±87 (N = 22) | |
| | R-pC | | | -584±175 (N = 23) | -446±93 (N = 22) | |
| | R-Shear | | | 983±318 (N = 23) | 726±147 (N = 22) | |
| | R-Phi (units in degrees) | | | 59±2 (N = 23) | 59±4 (N = 22) | |
| IG12 - mass=2.5kg; SVL=44.7 cm | SE-Postero-ventral | -431±122 (N = 19) | -468±117 (N = 18) | -541±306 (N = 18) | -336±434 (N = 2) | -504±121 (N = 17) |
| | SE-Ventral | 307±291 (N = 9) | | | | |
| | SE-R Anterior | 368±131 (N = 19) | | | | |
| | R-pT | | | | | |
| | R-pC | | | | | |
| | R-Shear | | | | | |
| | R-Phi (units in degrees) | | | | | |

| Animal | Gauge metric | FL-LEV | FL-COMP | FL-INC | CURV-INC | CURV-LEV |
|--------------------------------|--------------------------|--------------------|--------------------|--------------------|--------------------|--------------------|
| IG13 - mass=1.13 kg; SVL=34.67 | SE-Postero-ventral | 379±165 (N = 17) | 353±260 (N = 15) | 540±220 (N = 22) | 414±170 (N = 8) | 219±142 (N = 19) |
| | SE-Ventral | -164±85 (N = 17) | -154±86 (N = 15) | -140±113 (N = 22) | -126±54 (N = 8) | -173±126 (N = 19) |
| | SE-R Anterior | | | | | |
| | R-pT | | 170±119 (N = 18) | 196±89 (N = 22) | 146±67 (N = 8) | |
| | R-pC | | -270±126 (N = 18) | -317±132 (N = 22) | -278±152 (N = 8) | |
| | R-Shear | | 227±87 (N = 18) | 270±114 (N = 22) | 217±48 (N = 8) | |
| | R-Phi (units in degrees) | | | 36±16 (N = 22) | 44±18 (N = 8) | |
| IG14 - 1.36 kg; SVL=36.22 cm | SE-Postero-ventral | 325±167 (N = 17) | 537±212 (N = 15) | 672±283 (N = 25) | 1040±386 (N = 22) | 259±273 (N = 17) |
| | SE-Ventral | 288±107 (N = 17) | 429±94 (N = 15) | | | 246±128 (N = 17) |
| | SE-R Anterior | -324±188 (N = 17) | -446±313 (N = 15) | -422±175 (N = 25) | -414±176 (N = 22) | -283±284 (N = 17) |
| | R-pT | 867±241 (N = 17) | 987±330 (N = 15) | 1324±340 (N = 25) | 1712±457 (N = 22) | 1042±279 (N = 17) |
| | R-pC | -1016±373 (N = 17) | -1301±310 (N = 15) | -1430±381 (N = 25) | -1519±527 (N = 22) | -1167±337 (N = 17) |
| | R-Shear | 1801±654 (N = 17) | 2185±688 (N = 15) | 2648±699 (N = 25) | 2810±834 (N = 22) | 2166±594 (N = 17) |
| | R-Phi (units in degrees) | 53±43 (N = 17) | 47±7 (N = 15) | 50±3 (N = 25) | 51±5 (N = 22) | 43±4 (N = 17) |

Table S3. Total individual and interacting trackway factor influence on hindlimb (a) and forelimb (b) strain metrics. Type III ANOVA tests were performed, with *p*-value significance level indicated in the right column.

(a)

| Hindlimb | Factor | Degrees of Freedom | F value | Pr(>F) | |
|----------------------|----------------------|--------------------|----------|--------|-------|
| Maximum SE-R Dorsal | angle | (1, 330) | 35.196 | 0.000 | *** |
| | curvature | (1, 328) | 0.267 | 0.606 | |
| | stiffness | (1, 328) | 0.570 | 0.451 | |
| | mass | (1, 3) | 0.401 | 0.573 | |
| | angle:curvature | (1, 328) | 3.531 | 0.061 | |
| | angle:mass | (1, 329) | 50.869 | 0.000 | *** |
| | curvature:mass | (1, 328) | 0.452 | 0.502 | |
| | stiffness:mass | (1, 328) | 1.231 | 0.268 | |
| | angle:curvature:mass | (1, 328) | 3.984 | 0.047 | * |
| | Minimum SE-R Dorsal | angle | (1, 331) | 0.900 | 0.343 |
| curvature | | (1, 328) | 0.035 | 0.852 | |
| stiffness | | (1, 328) | 2.276 | 0.132 | |
| mass | | (1, 3) | 0.863 | 0.433 | |
| angle:curvature | | (1, 328) | 2.453 | 0.118 | |
| angle:mass | | (1, 331) | 0.380 | 0.538 | |
| curvature:mass | | (1, 328) | 0.009 | 0.924 | |
| stiffness:mass | | (1, 328) | 1.703 | 0.193 | |
| angle:curvature:mass | | (1, 328) | 3.079 | 0.080 | |
| Minimum R-pC | | angle | (1, 268) | 22.075 | 0.000 |
| | curvature | (1, 266) | 0.616 | 0.433 | |
| | stiffness | (1, 269) | 1.728 | 0.190 | |
| | mass | (1, 3) | 0.112 | 0.762 | |
| | angle:curvature | (1, 266) | 10.781 | 0.001 | ** |
| | angle:mass | (1, 267) | 32.732 | 0.000 | *** |
| | curvature:mass | (1, 266) | 0.095 | 0.758 | |
| | stiffness:mass | (1, 269) | 2.417 | 0.121 | |
| | angle:curvature:mass | (1, 266) | 12.255 | 0.001 | *** |
| | Maximum R-pT | angle | (1, 259) | 0.018 | 0.894 |
| curvature | | (1, 268) | 0.088 | 0.767 | |
| stiffness | | (1, 252) | 0.463 | 0.497 | |
| mass | | (1, 3) | 0.500 | 0.533 | |
| angle:curvature | | (1, 268) | 0.699 | 0.404 | |
| angle:mass | | (1, 264) | 0.027 | 0.870 | |
| curvature:mass | | (1, 268) | 0.000 | 0.992 | |
| stiffness:mass | | (1, 259) | 0.392 | 0.532 | |
| angle:curvature:mass | | (1, 268) | 1.401 | 0.238 | |
| Maximum R-Shear | | angle | (1, 263) | 0.063 | 0.802 |

| | | | | | |
|---------------------|----------------------|----------|--------|-------|-----|
| | curvature | (1, 266) | 2.932 | 0.088 | |
| | stiffness | (1, 266) | 0.930 | 0.336 | |
| | mass | (1, 2) | 0.104 | 0.773 | |
| | angle:curvature | (1, 266) | 0.292 | 0.590 | |
| | angle:mass | (1, 264) | 0.242 | 0.623 | |
| | curvature:mass | (1, 266) | 2.163 | 0.143 | |
| | stiffness:mass | (1, 266) | 0.740 | 0.391 | |
| | angle:curvature:mass | (1, 266) | 0.112 | 0.738 | |
| Maximum SE-Ventral | angle | (1, 292) | 14.937 | 0.000 | *** |
| | curvature | (1, 294) | 3.807 | 0.052 | |
| | stiffness | (1, 293) | 6.328 | 0.012 | * |
| | mass | (1, 3) | 0.817 | 0.440 | |
| | angle:curvature | (1, 294) | 1.271 | 0.261 | |
| | angle:mass | (1, 294) | 12.143 | 0.001 | *** |
| | curvature:mass | (1, 293) | 2.927 | 0.088 | |
| | stiffness:mass | (1, 293) | 5.245 | 0.023 | * |
| | angle:curvature:mass | (1, 293) | 0.870 | 0.352 | |
| Minimum SE-Ventral | angle | (1, 289) | 16.872 | 0.000 | *** |
| | curvature | (1, 294) | 7.790 | 0.006 | ** |
| | stiffness | (1, 292) | 1.389 | 0.239 | |
| | mass | (1, 2) | 3.024 | 0.216 | |
| | angle:curvature | (1, 293) | 8.354 | 0.004 | ** |
| | angle:mass | (1, 292) | 28.015 | 0.000 | *** |
| | curvature:mass | (1, 293) | 11.937 | 0.001 | *** |
| | stiffness:mass | (1, 292) | 2.105 | 0.148 | |
| | angle:curvature:mass | (1, 293) | 10.569 | 0.001 | ** |
| Maximum SE-Anterior | angle | (1, 204) | 40.386 | 0.000 | *** |
| | curvature | (1, 331) | 4.126 | 0.043 | * |
| | stiffness | (1, 332) | 1.278 | 0.259 | |
| | mass | (1, 1) | 23.993 | 0.078 | |
| | angle:curvature | (1, 331) | 0.047 | 0.829 | |
| | angle:mass | (1, 249) | 30.460 | 0.000 | *** |
| | curvature:mass | (1, 331) | 3.453 | 0.064 | |
| | stiffness:mass | (1, 332) | 1.067 | 0.302 | |
| | angle:curvature:mass | (1, 331) | 0.048 | 0.826 | |
| Minimum SE-Anterior | angle | (1, 334) | 4.948 | 0.027 | * |
| | curvature | (1, 333) | 1.048 | 0.307 | |
| | stiffness | (1, 333) | 0.252 | 0.616 | |
| | mass | (1, 3) | 0.014 | 0.913 | |

| | | | | | |
|---|----------------------|----------|-------|-------|--|
| | angle:curvature | (1, 333) | 0.092 | 0.762 | |
| | angle:mass | (1, 334) | 3.437 | 0.065 | |
| | curvature:mass | (1, 333) | 1.471 | 0.226 | |
| | stiffness:mass | (1, 333) | 0.392 | 0.532 | |
| | angle:curvature:mass | (1, 333) | 0.165 | 0.685 | |
| * – <0.05 P-VALUE; ** – <0.01 P-VALUE; *** – <0.001 P-VALUE | | | | | |

(b)

| Forelimb | Factor | Degrees of Freedom | F value | Pr(>F) | |
|-----------------------|-----------------------|--------------------|----------|--------|-------|
| Maximum SE-R Anterior | angle | (1, 314) | 59.346 | 0.000 | *** |
| | curvature | (1, 314) | 11.581 | 0.001 | *** |
| | stiffness | (1, 313) | 1.021 | 0.313 | |
| | mass | (1, 5) | 1.774 | 0.239 | |
| | angle:curvature | (1, 313) | 15.193 | 0.000 | *** |
| | angle:mass | (1, 314) | 43.746 | 0.000 | *** |
| | curvature:mass | (1, 314) | 13.754 | 0.000 | *** |
| | stiffness:mass | (1, 313) | 0.675 | 0.412 | |
| | angle:curvature:mass | (1, 313) | 16.716 | 0.000 | *** |
| | Minimum SE-R Anterior | angle | (1, 313) | 0.693 | 0.406 |
| curvature | | (1, 312) | 0.423 | 0.516 | |
| stiffness | | (1, 311) | 2.463 | 0.118 | |
| mass | | (1, 5) | 0.715 | 0.440 | |
| angle:curvature | | (1, 311) | 0.068 | 0.794 | |
| angle:mass | | (1, 313) | 0.285 | 0.594 | |
| curvature:mass | | (1, 312) | 0.270 | 0.604 | |
| stiffness:mass | | (1, 312) | 1.874 | 0.172 | |
| angle:curvature:mass | | (1, 311) | 0.080 | 0.777 | |
| Minimum R-pC | | angle | (1, 270) | 1.234 | 0.268 |
| | curvature | (1, 269) | 1.301 | 0.255 | |
| | stiffness | (1, 269) | 14.913 | 0.000 | *** |
| | mass | (1, 2) | 0.020 | 0.900 | |
| | angle:curvature | (1, 269) | 7.655 | 0.006 | ** |
| | angle:mass | (1, 270) | 0.056 | 0.813 | |
| | curvature:mass | (1, 270) | 2.115 | 0.147 | |
| | stiffness:mass | (1, 269) | 12.270 | 0.001 | *** |
| | angle:curvature:mass | (1, 270) | 6.873 | 0.009 | ** |
| | Maximum R-pT | angle | (1, 270) | 3.994 | 0.047 |
| curvature | | (1, 270) | 24.148 | 0.000 | *** |
| stiffness | | (1, 269) | 12.538 | 0.000 | *** |
| mass | | (1, 2) | 0.664 | 0.499 | |
| angle:curvature | | (1, 270) | 46.013 | 0.000 | *** |
| angle:mass | | (1, 270) | 11.463 | 0.001 | *** |
| curvature:mass | | (1, 270) | 31.791 | 0.000 | *** |
| stiffness:mass | | (1, 269) | 11.813 | 0.001 | *** |
| angle:curvature:mass | | (1, 270) | 48.462 | 0.000 | *** |
| Maximum R-Shear | | angle | (1, 270) | 0.721 | 0.397 |

| | | | | | |
|---------------------------|----------------------|----------|--------|-------|-----|
| | curvature | (1, 269) | 1.835 | 0.177 | |
| | stiffness | (1, 269) | 16.804 | 0.000 | *** |
| | mass | (1, 2) | 0.096 | 0.785 | |
| | angle:curvature | (1, 269) | 12.108 | 0.001 | *** |
| | angle:mass | (1, 270) | 0.006 | 0.938 | |
| | curvature:mass | (1, 269) | 3.197 | 0.075 | |
| | stiffness:mass | (1, 269) | 14.942 | 0.000 | *** |
| | angle:curvature:mass | (1, 269) | 10.837 | 0.001 | ** |
| Maximum SE-Posteroventral | angle | (1, 513) | 1.186 | 0.277 | |
| | curvature | (1, 513) | 7.329 | 0.007 | ** |
| | stiffness | (1, 512) | 1.146 | 0.285 | |
| | mass | (1, 4) | 1.140 | 0.340 | |
| | angle:curvature | (1, 513) | 4.561 | 0.033 | * |
| | angle:mass | (1, 513) | 3.057 | 0.081 | |
| | curvature:mass | (1, 513) | 8.737 | 0.003 | ** |
| | stiffness:mass | (1, 512) | 1.293 | 0.256 | |
| | angle:curvature:mass | (1, 513) | 13.009 | 0.000 | *** |
| Minimum SE-Posteroventral | angle | (1, 512) | 0.298 | 0.585 | |
| | curvature | (1, 512) | 8.653 | 0.003 | ** |
| | stiffness | (1, 512) | 3.643 | 0.057 | |
| | mass | (1, 4) | 2.662 | 0.175 | |
| | angle:curvature | (1, 512) | 5.405 | 0.020 | * |
| | angle:mass | (1, 512) | 0.303 | 0.582 | |
| | curvature:mass | (1, 512) | 5.035 | 0.025 | * |
| | stiffness:mass | (1, 512) | 4.572 | 0.033 | * |
| | angle:curvature:mass | (1, 512) | 5.093 | 0.024 | * |
| Maximum SE-Ventral | angle | (1, 315) | 9.609 | 0.002 | ** |
| | curvature | (1, 315) | 12.713 | 0.000 | *** |
| | stiffness | (1, 315) | 1.225 | 0.269 | |
| | mass | (1, 166) | 8.346 | 0.004 | ** |
| | angle:curvature | (1, 315) | 13.778 | 0.000 | *** |
| | angle:mass | (1, 315) | 11.621 | 0.001 | *** |
| | curvature:mass | (1, 315) | 13.201 | 0.000 | *** |
| | stiffness:mass | (1, 312) | 0.732 | 0.393 | |
| | angle:curvature:mass | (1, 315) | 14.204 | 0.000 | *** |
| Minimum SE-Ventral | angle | (1, 313) | 0.158 | 0.691 | |
| | curvature | (1, 310) | 0.041 | 0.840 | |
| | stiffness | (1, 249) | 1.008 | 0.316 | |
| | mass | (1, 260) | 0.000 | 0.989 | |

| | | | | | |
|---|----------------------|----------|-------|-------|--|
| | angle:curvature | (1, 312) | 0.146 | 0.702 | |
| | angle:mass | (1, 312) | 0.177 | 0.674 | |
| | curvature:mass | (1, 310) | 0.067 | 0.796 | |
| | stiffness:mass | (1, 202) | 0.584 | 0.446 | |
| | angle:curvature:mass | (1, 312) | 0.176 | 0.675 | |
| * – <0.05 P-VALUE; ** – <0.01 P-VALUE; *** – <0.001 P-VALUE | | | | | |